6th China–Japan–Korea Joint Symposium on Optimization of Structural and Mechanical Systems
June 22-25, 2010, Kyoto, Japan

Shape Optimization of Shells Considering Quantity of Local Geometric Characteristics

Shinnosuke Fujita [1] **and Makoto Ohsaki** [2]

[1]Kanebako Structural Engineers, 4-5-18-3F, Kami-Ohsaki, Shinagawa, Tokyo, 141-0021, Japan
fujita@kanebako-se.co.jp
[2]Dept. of Architecture, Hiroshima University, Higashi-Hiroshima 739-8527, Japan
ohsaki@hiroshima-u.ac.jp

Abstract
A method is presented for shape optimization of shell surfaces considering local geometric characteristics that represent aesthetic aspect and the constructability of the surface. Mechanical performance is also considered in the problem formulation. The surface shape is modeled using Bézier surface to reduce the number of variables, while the ability to generate moderately complex shape is maintained. The developable surface that has high constructability is created by imposing appropriate algebraic invariants constraints. A measure of roundness is also defined using the invariant, and a set of trade-off designs between roundness and mechanical rationality is generated using the constraint approach of multiobjective programming. It is shown that the sensitivity coefficients of the algebraic invariants can be explicitly derived with respect to the locations of the control points o the Bźier surface.

Keywords: Shape optimization, Sensitivity analysis, Algebraic invariants, Multiobjective programming, Free-form shell

1. Introduction

By contrast to the traditional regular shells such as spherical shell, cylindrical shell, and hyperbolic paraboloid (HP) shell, so called free-form shells [1–3] are extensively designed for long-span structures for stadiums and arenas. It is mainly due to advances of computer technologies as well as the developments of structural materials and construction methods. Free-form shells are described using parametric surfaces, e.g., Bézier surface and non-uniform rational B-spline (NURBS) surface [4].

Using a parametric surface, the number of design variables can be reduced, while the ability of generating moderately complex shape is maintained. Therefore, the parametric representation is effectively used for shape optimization of surfaces, which has been mainly developed in the fields of mechanical engineering and aeronautical engineering [5]. For application to spatial structures, shape optimization of shell roofs has been extensively studied since 1990s. Ramm et al. [2] optimized shapes of shells under buckling constraints, where Bézier surface is used for modeling the surface. However, in those studies, the performance measures that are important in the field of architectural engineering are not considered.

One of the important aspects in design of shell roofs is that their shapes are basically designed based on the preference and experience of the architects and structural designers. It may be possible for the designer to assign the most desired shape explicitly. However, the mechanical behavior of a shell with non-regular shape is complicated, and it is very difficult for an architect to decide a feasible shape of a real-world structure based on his/her experience and intuition.

Ohsaki et al. [6] presented a shape optimization approach for latticed shells defined using a triangular Bézier patch. Ohsaki and Hayashi [7] defined a roundness metric for shape optimization of ribbed shells. Ohsaki et al. [8] developed a multiobjective programming approach to design of round arches and shells based on direct assignment of the center of curvature. However, in these approaches, only global properties can be controlled, although there are local measures of geometry to be considered by the designers.

The authors developed a new approach to shape optimization of shells modeled using Bézier surface [9]. The strain energy is used to represent the mechanical performance, and the local geometrical characteristics are quantified by algebraic invariants of the surface representing curvature, convexity, gradient, etc. The requirement for developability of the surface is incorporated as the constraints on the principal curvature. However, the effectiveness of the approach was not fully appreciated, because the tensor product Bézier surface was used for a shell with rectangular plan.

In this study, we extend the authors' approach to utilize triangular Bézier patches that can model a shell with irregular plan. It is shown that the sensitivity coefficients of the algebraic invariants can be explicitly derived with respect to the locations of the control points of the Bézier surface. A new invariant is presented for the roundness of the surface. A multiobjective programming problem is solved using the constraint approach to generate a set of Pareto optimal solutions as a trade-off between mechanical efficiency and roundness. The effectiveness of the proposed approach is demonstrated through several numerical examples, and the characteristics of the optimal shapes under various constraints are discussed.

2. Shape representation by Bézier surface

The number of variables for optimization can be drastically reduced without sacrificing smoothness and complexity of the surface using the Bézier surface. Moreover, the basis functions of Bézier surface can be expressed explicitly with respect to the coordinates of the control points, which enables us to carry out sensitivity analysis of the algebraic invariants analytically. The Bézier surfaces are classified into tensor product Bézier surface and triangular Bézier surface. Since the latter is more suitable for modeling a surface with irregular plan, the shape of shell surface is described here using a Bézier surface consisting of triangular Bézier patches, which have control polygons with triangular units.

The point $\boldsymbol{S}_n(u,v)$ on a triangular Bézier surface in the 3-dimensional space (x,y,z) is defined with parameters $u, v \in [0,1](u+v \leq 1)$ as

$$\boldsymbol{S}_n(u,v) = \begin{pmatrix} x(u,v) \\ y(u,v) \\ z(u,v) \end{pmatrix} = \sum_{i=0}^{n}\sum_{j=0}^{n-i} \boldsymbol{q}_{ij} B_{n,ij}(u,v), \qquad B_{n,ij}(u,v) = \frac{n!}{i!\,j!(n-i-j)!} u^i v^j (1-u-v)^{n-i-j}, \quad (0^0 = 0! = 1) \tag{1}$$

where $\boldsymbol{q}_{ij} = [q_{x,ij}, q_{y,ij}, q_{z,ij}]^\top$ is the location vector of the control point, $B_{n,ij}(u,v)$ is the bivariate Bernstein basis function, and n is the order of the surface. The vectors consisting of x-, y-, and z-coordinates of all control points are denoted by $\boldsymbol{q}_x$, $\boldsymbol{q}_y$, and $\boldsymbol{q}_z$, respectively; e.g., $\boldsymbol{q}_x$ is defined as

$$\boldsymbol{q}_x = (q_{x,00}, \cdots, q_{x,n0}, \cdots, q_{x,0i}, \cdots, q_{x(n-i)i}, \cdots, q_{x,0n})^\top \tag{2}$$

3. Algebraic invariants

3. 1. Definition of tensors and vectors

We use the six algebraic invariants β_0,β_1,β_2,γ_1,γ_2, and γ_3 proposed by Iri et al. [10] for representing the geographical properties. Here, we regard the z-coordinate of the Bézier surface as the altitude of the geographical representation.

In the following, the covariant and the contravariant components are indicated by the subscript and superscript, respectively. The components of the covariant gradient vector $\underline{\boldsymbol{z}}$, the covariant hessian $\underline{\boldsymbol{h}}$, and the covariant metric tensor $\underline{\boldsymbol{g}}$ of the surface $\boldsymbol{S}_n(u,v)$ are defined as

$$\underline{\boldsymbol{z}} = \begin{pmatrix} z_u \\ z_v \end{pmatrix}, \qquad \underline{\boldsymbol{h}} = \begin{pmatrix} h_{uu} & h_{uv} \\ h_{vu} & h_{vv} \end{pmatrix}, \qquad \underline{\boldsymbol{g}} = \begin{pmatrix} g_{uu} & g_{uv} \\ g_{vu} & g_{vv} \end{pmatrix} \tag{3}$$

which are obtained from

$$z_s = \frac{\partial z(u,v)}{\partial s}, \qquad h_{st} = \frac{\partial^2 z(u,v)}{\partial s \partial t}, \qquad g_{st} = \frac{\partial \boldsymbol{S}_n(u,v)}{\partial s}^\top \frac{\partial \boldsymbol{S}_n(u,v)}{\partial t}, \quad s,t \in \{u,v\} \tag{4}$$

Let $\overline{\boldsymbol{z}}$ and $\overline{\boldsymbol{g}}$ denote the contravariant gradient of the z-coordinate and the contravariant metric tensor, respectively. Then the following relations hold:

$$\overline{\boldsymbol{g}} = \underline{\boldsymbol{g}}^{-1}, \qquad \overline{\boldsymbol{z}} = \overline{\boldsymbol{g}}\underline{\boldsymbol{z}}, \qquad \underline{\boldsymbol{z}} = \underline{\boldsymbol{g}}\overline{\boldsymbol{z}} \tag{5}$$

Furthermore, we define the following contravariant vector $\tilde{\boldsymbol{z}}$ and tensor $\tilde{\boldsymbol{E}}$:

$$\tilde{\boldsymbol{z}} = \begin{pmatrix} \tilde{z}^u \\ \tilde{z}^v \end{pmatrix} = \tilde{\boldsymbol{E}}\underline{\boldsymbol{z}}, \qquad \tilde{\boldsymbol{E}} = \begin{pmatrix} 0 & 1 \\ -1 & 1 \end{pmatrix} \tag{6}$$

The inner product of a covariant vector and a contravariant vector as well as the bilinear form with respect to a second order covariant/contravariant tensor and a contravariant/covariant vector are invariant with respect to the definition of the parameter of the surface. Hence, β- and γ-invariants are defined as follows[10]:

$$\beta_0 = \sum_{\xi=s,t}\sum_{\lambda=s,t} g^{\xi\lambda} z_\xi z_\lambda = \sum_{\xi=s,t} z^\xi z_\xi \ (\geq 0), \qquad \beta_1 = \sum_{\xi=s,t}\sum_{\lambda=s,t} h_{\lambda\xi} g^{\xi\lambda}, \qquad \beta_2 = \frac{1}{2\det(\underline{\boldsymbol{g}})} \sum_{\xi=s,t}\sum_{\lambda=s,t}\sum_{\mu=s,t}\sum_{\nu=s,t} h_{\nu\lambda} h_{\mu\xi} \tilde{E}^{\xi\lambda} \tilde{E}^{\mu\nu} \tag{7}$$

$$\gamma_1 = \sum_{\lambda=s,t}\sum_{\xi=s,t} h_{\lambda\xi} z^\xi z^\lambda, \qquad \gamma_2 = \sum_{\lambda=s,t}\sum_{\xi=s,t} h_{\lambda\xi} \tilde{z}^\xi z^\lambda = \sum_{\lambda=s,t}\sum_{\xi=s,t} h_{\lambda\xi} z^\xi \tilde{z}^\lambda, \qquad \gamma_3 = \frac{1}{\det(\underline{\boldsymbol{g}})} \sum_{\lambda=s,t}\sum_{\xi=s,t} h_{\lambda\xi} \tilde{z}^\xi \tilde{z}^\lambda \tag{8}$$

These equations can also be expressed in a matrix form as follows:

$$\beta_0 = \underline{\boldsymbol{z}}^\top \overline{\boldsymbol{z}} = \underline{\boldsymbol{z}}^\top \overline{\boldsymbol{g}}\underline{\boldsymbol{z}}, \qquad \beta_1 = \boldsymbol{e}_1^\top \underline{\boldsymbol{h}}\overline{\boldsymbol{g}}\boldsymbol{e}_1 + \boldsymbol{e}_2^\top \underline{\boldsymbol{h}}\overline{\boldsymbol{g}}\boldsymbol{e}_2, \quad \boldsymbol{e}_1 = (\,1\ \ 0\,)^\top, \boldsymbol{e}_2 = (\,0\ \ 1\,)^\top, \qquad \beta_2 = \frac{\det(\underline{\boldsymbol{h}})}{\det(\underline{\boldsymbol{g}})} \tag{9}$$

$$\gamma_1 = \overline{\boldsymbol{z}}^\top \underline{\boldsymbol{h}}\overline{\boldsymbol{z}} = \overline{\boldsymbol{g}}^\top \underline{\boldsymbol{z}}^\top \underline{\boldsymbol{h}}\overline{\boldsymbol{g}}\underline{\boldsymbol{z}}, \qquad \gamma_2 = \overline{\boldsymbol{z}}^\top \underline{\boldsymbol{h}}\tilde{\boldsymbol{z}} = \overline{\boldsymbol{g}}^\top \underline{\boldsymbol{z}}^\top \underline{\boldsymbol{h}}\tilde{\boldsymbol{E}}\underline{\boldsymbol{z}}, \qquad \gamma_3 = \frac{\tilde{\boldsymbol{E}}^\top \underline{\boldsymbol{z}}^\top \underline{\boldsymbol{h}}\tilde{\boldsymbol{E}}\underline{\boldsymbol{z}}}{\det(\underline{\boldsymbol{g}})} \tag{10}$$

3. 2. Surface properties based on six algebraic invariants

The six algebraic invariants $\beta_0, \beta_1, \beta_2, \gamma_1, \gamma_2$, and γ_3, defined using the vectors and tensors given in Sec.3. 1., are used for quantitative evaluation of the surface properties. The local properties in the neighborhood of a point P on the surface are characterized by the invariants as follows:

$\underline{\beta_2 > 0}$ The contours in the neighborhood of P are coaxial (part of) similar ellipses. The shape is locally concave if $\beta_1 > 0$, and locally convex if $\beta_1 < 0$.

$\underline{\beta_2 < 0}$ The contours in the neighborhood of P are (part of) coaxial hyperbolas. Locally, the surface is convex in some directions and concave in others. There are special directions in which the contour lines are straight.

$\underline{\beta_2 = 0}$ One of the principal curvatures is 0. Furthermore, the other principal curvature is positive if $\beta_1 > 0$; and negative if $\beta_1 < 0$; and 0 if $\beta_1 = 0$ that means a locally flat surface.

$\underline{\beta_0 = 0}$ P is a critical point (locally maximum/minimum value of z-coordinate).

$\underline{\gamma_2 = 0}$ Direction of gradient vector coincides with one of the principal direction, and the surface near P is locally cylindrical and concave in one principal direction if $|\gamma_1| < |\gamma_3|$ and $\gamma_3 > 0$; whereas it is locally cylindrical and convex in one principal direction if $|\gamma_1| < |\gamma_3|$ and $\gamma_3 < 0$.

Moreover, $\beta_1/2$ is the mean curvature, β_2 is the Gaussian curvature, γ_1/β_0 is the curvature in the steepest descent direction, and γ_3/β_0 is the curvature in its perpendicular direction.

In view of constructability, it is desirable that the surface can be developed to a plane without expansion or contraction. Such surface is called developable surface, which is characterized by vanishing Gaussian curvature. Therefore, to generate a developable surface, the constraint $\beta_2 = 0$ should be satisfied at any point on the surface.

We define an additional invariant for characterizing roundness of the surface as follows.

$$\alpha == \frac{1}{4}(\kappa_1 - \kappa_2)^2 \tag{11}$$

where κ_1 and κ_2 are the principal curvatures, respectively. A small value of α corresponds to a locally spherical surface.

4. Sensitivity analysis

In the following numerical examples, the sequential quadratic programming, which is categorized as a gradient-based method and available from a software library in SNOPT [11], is used for optimization. Therefore, sensitivity coefficients of the invariants are needed with respect to the locations of the control points. For instance, for obtaining sensitivity coefficients of the algebraic invariants with respect to the z-coordinates $\boldsymbol{q}_z$ of the control points, those of the gradient, Hessian, and the metric tensor are needed. Owing to the representation of the surface using triangular Bézier patch, these sensitivity coefficients can be derived explicitly as follows:

$$\frac{\partial \underline{\boldsymbol{z}}}{\partial q_{z,ij}} = \begin{pmatrix} \dfrac{\partial z_u}{\partial q_{z,ij}} \\ \dfrac{\partial z_v}{\partial q_{z,ij}} \end{pmatrix} = \begin{pmatrix} \dfrac{\partial B_{n,ij}(u,v)}{\partial u} \\ \dfrac{\partial B_{n,ij}(u,v)}{\partial v} \end{pmatrix} \tag{12}$$

$$\frac{\partial \underline{\boldsymbol{h}}}{\partial q_{z,ij}} = \begin{pmatrix} \dfrac{\partial h_{uu}}{\partial q_{z,ij}} & \dfrac{\partial h_{uv}}{\partial q_{z,ij}} \\ \dfrac{\partial h_{vu}}{\partial q_{z,ij}} & \dfrac{\partial h_{vv}}{\partial q_{z,ij}} \end{pmatrix} = \begin{pmatrix} \dfrac{\partial^2 B_{n,ij}(u,v)}{\partial u^2} & \dfrac{\partial^2 B_{n,ij}(u,v)}{\partial u \partial v} \\ \dfrac{\partial^2 B_{n,ij}(u,v)}{\partial u \partial v} & \dfrac{\partial^2 B_{n,ij}(u,v)}{\partial v^2} \end{pmatrix} \tag{13}$$

$$\frac{\partial \underline{\boldsymbol{g}}}{\partial q_{z,ij}} = \begin{pmatrix} \dfrac{\partial g_{uu}}{\partial q_{z,ij}} & \dfrac{\partial g_{uv}}{\partial q_{z,ij}} \\ \dfrac{\partial g_{vu}}{\partial q_{z,ij}} & \dfrac{\partial g_{vv}}{\partial q_{z,ij}} \end{pmatrix} = \begin{pmatrix} 2z_u \dfrac{\partial z_u}{\partial q_{z,ij}} & \dfrac{\partial z_u}{\partial q_{z,ij}} z_v + z_u \dfrac{\partial z_v}{\partial q_{z,ij}} \\ \dfrac{\partial z_u}{\partial q_{z,ij}} z_v + z_u \dfrac{\partial z_v}{\partial q_{z,ij}} & 2z_v \dfrac{\partial z_v}{\partial q_{z,ij}} \end{pmatrix} \tag{14}$$

4. 1. Sensitivity of β invariants

The next equation is provided by partial differentiation of Eq. (9) in $q_{z,ij}$ as follows:

$$\frac{\partial \beta_0}{\partial q_{z,ij}} = \frac{\partial \underline{\boldsymbol{z}}}{\partial q_{z,ij}}^{\top} \overline{\boldsymbol{g}}\underline{\boldsymbol{z}} + \underline{\boldsymbol{z}}^{\top} \frac{\partial \overline{\boldsymbol{g}}}{\partial q_{z,ij}} \underline{\boldsymbol{z}} + \underline{\boldsymbol{z}}^{\top} \overline{\boldsymbol{g}} \frac{\partial \underline{\boldsymbol{z}}}{\partial q_{z,ij}} \tag{15}$$

$$\frac{\partial \beta_1}{\partial q_{z,ij}} = \boldsymbol{e}_1^{\top} \frac{\partial \underline{\boldsymbol{h}}}{\partial q_{z,ij}} \overline{\boldsymbol{g}} \boldsymbol{e}_1 + \boldsymbol{e}_1^{\top} \underline{\boldsymbol{h}} \frac{\partial \overline{\boldsymbol{g}}}{\partial q_{z,ij}} \boldsymbol{e}_1 + \boldsymbol{e}_2^{\top} \frac{\partial \underline{\boldsymbol{h}}}{\partial q_{z,ij}} \overline{\boldsymbol{g}} \boldsymbol{e}_2 + \boldsymbol{e}_2^{\top} \underline{\boldsymbol{h}} \frac{\partial \overline{\boldsymbol{g}}}{\partial q_{z,ij}} \boldsymbol{e}_2 \tag{16}$$

$$\frac{\partial \beta_2}{\partial q_{z,ij}} = \frac{\partial \det(\underline{\boldsymbol{h}})}{\partial q_{z,ij}} \det(\underline{\boldsymbol{g}})^{-1} + \det(\underline{\boldsymbol{h}}) \frac{\partial \det(\underline{\boldsymbol{g}})^{-1}}{\partial q_{z,ij}} \tag{17}$$

It is difficult to calculate $\dfrac{\partial \overline{\boldsymbol{g}}}{\partial q_{z,ij}}$ explicitly. Therefore we obtain the next equation by partial differentiation of $\overline{\boldsymbol{g}}\underline{\boldsymbol{g}} = \boldsymbol{I}$ in $q_{z,ij}$:

$$\frac{\partial \overline{\boldsymbol{g}}}{\partial q_{z,ij}} \underline{\boldsymbol{g}} + \overline{\boldsymbol{g}} \frac{\partial \underline{\boldsymbol{g}}}{\partial q_{z,ij}} = 0 \tag{18}$$

Therefore, the next expression holds:

$$\frac{\partial \overline{\boldsymbol{g}}}{\partial q_{z,ij}} = -\overline{\boldsymbol{g}} \frac{\partial \underline{\boldsymbol{g}}}{\partial q_{z,ij}} \overline{\boldsymbol{g}} \tag{19}$$

And Eq. (17) is obtained from

$$\frac{\partial \det(\underline{\boldsymbol{h}})}{\partial q_{z,ij}} = \frac{\partial h_{ss}}{\partial q_{z,ij}} h_{tt} + h_{ss} \frac{\partial h_{tt}}{\partial q_{z,ij}} - 2h_{st} \frac{\partial h_{st}}{\partial q_{z,ij}} \tag{20}$$

$$\frac{\partial \det(\underline{\boldsymbol{g}})^{-1}}{\partial q_{z,ij}} = \frac{\partial (g_{ss}g_{tt} - g_{st}^2)^{-1}}{\partial q_{z,ij}} = -\frac{1}{(g_{ss}g_{tt} - g_{st}^2)^2} \left(\frac{\partial g_{ss}}{\partial q_{z,ij}} g_{tt} + g_{ss} \frac{\partial g_{tt}}{\partial q_{z,ij}} - 2g_{st} \frac{\partial g_{st}}{\partial q_{z,ij}} \right) \tag{21}$$

4. 2. Sensitivity of γ invariants

The next equation is provided by considering partial differentiation of Eq. (10) in $q_{z,ij}$ as follows:

$$\frac{\partial \gamma_1}{\partial q_{z,ij}} = \frac{\partial \underline{\boldsymbol{z}}}{\partial q_{z,ij}}^{\top} \overline{\boldsymbol{g}}\underline{\boldsymbol{h}}\overline{\boldsymbol{g}}\underline{\boldsymbol{z}} + \underline{\boldsymbol{z}}^{\top} \frac{\partial \overline{\boldsymbol{g}}}{\partial q_{z,ij}} \underline{\boldsymbol{h}}\overline{\boldsymbol{g}}\underline{\boldsymbol{z}} + \underline{\boldsymbol{z}}^{\top} \overline{\boldsymbol{g}} \frac{\partial \underline{\boldsymbol{h}}}{\partial q_{z,ij}} \overline{\boldsymbol{g}}\underline{\boldsymbol{z}} + \underline{\boldsymbol{z}}^{\top} \overline{\boldsymbol{g}}\underline{\boldsymbol{h}} \frac{\partial \overline{\boldsymbol{g}}}{\partial q_{z,ij}} \underline{\boldsymbol{z}} + \underline{\boldsymbol{z}}^{\top} \overline{\boldsymbol{g}}\underline{\boldsymbol{h}}\overline{\boldsymbol{g}} \frac{\partial \underline{\boldsymbol{z}}}{\partial q_{z,ij}} \tag{22}$$

$$\frac{\partial \gamma_2}{\partial q_{z,ij}} = \frac{\partial \underline{\boldsymbol{z}}}{\partial q_{z,ij}}^{\top} \overline{\boldsymbol{g}}\underline{\boldsymbol{h}}\tilde{\boldsymbol{E}}\underline{\boldsymbol{z}} + \underline{\boldsymbol{z}}^{\top} \frac{\partial \overline{\boldsymbol{g}}}{\partial q_{z,ij}} \underline{\boldsymbol{h}}\tilde{\boldsymbol{E}}\underline{\boldsymbol{z}} + \underline{\boldsymbol{z}}^{\top} \overline{\boldsymbol{g}} \frac{\partial \underline{\boldsymbol{h}}}{\partial q_{z,ij}} \tilde{\boldsymbol{E}}\underline{\boldsymbol{z}} + \underline{\boldsymbol{z}}^{\top} \overline{\boldsymbol{g}}\underline{\boldsymbol{h}}\tilde{\boldsymbol{E}} \frac{\partial \underline{\boldsymbol{z}}}{\partial q_{z,ij}} \tag{23}$$

$$\frac{\partial \gamma_3}{\partial q_{z,ij}} = \frac{\partial \underline{\boldsymbol{z}}}{\partial q_{z,ij}}^{\top} \tilde{\boldsymbol{E}}\underline{\boldsymbol{h}}\tilde{\boldsymbol{E}}\underline{\boldsymbol{z}} \det(\underline{\boldsymbol{g}})^{-1} + \underline{\boldsymbol{z}}^{\top} \tilde{\boldsymbol{E}} \frac{\partial \underline{\boldsymbol{h}}}{\partial q_{z,ij}} \tilde{\boldsymbol{E}}\underline{\boldsymbol{z}} \det(\underline{\boldsymbol{g}})^{-1} + \underline{\boldsymbol{z}}^{\top} \tilde{\boldsymbol{E}}\underline{\boldsymbol{h}}\tilde{\boldsymbol{E}} \frac{\partial \underline{\boldsymbol{z}}}{\partial q_{z,ij}} \det(\underline{\boldsymbol{g}})^{-1} + \underline{\boldsymbol{z}}^{\top} \tilde{\boldsymbol{E}}\underline{\boldsymbol{h}}\tilde{\boldsymbol{E}}\underline{\boldsymbol{z}} \frac{\partial \det(\underline{\boldsymbol{g}})^{-1}}{\partial q_{z,ij}} \tag{24}$$

5. Bézier surface with triangular plan

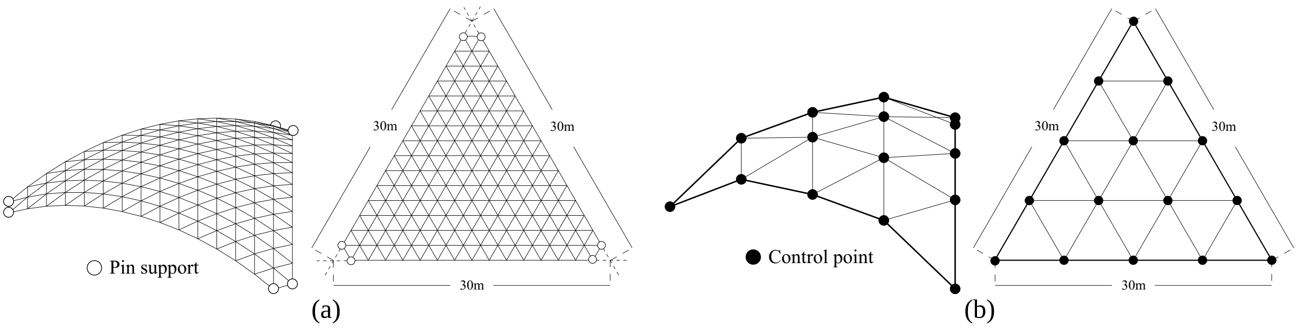

Figure 1 : Shell surface with triangular plan (Model 1); (a) plan and diagonal view, (b) Bézier patch and control points.

Consider first a shell surface with triangular plan (Model 1) that consists of a Bézier surface with triangular plan as shown in Figure 1. The shell is pin-supported at the three corners; however, there exist two supports at each corner, as shown in blank circles in Figure 1, to prevent stress concentration. The span length is 30 m and the radius of curvature is 17.06

m, which result in the rise of 4.84 m. The middle surface of shell is modeled using the triangular Bézier patch of order 5. The z-coordinates of all the 15 control points, as shown in filled circles, are chosen as variables, while the locations of the supports are fixed by assigning the constraints. The shell is discretized to triangular finite elements for static analysis. The constant-strain element [12] is used for in-plane deformation, and the non-conforming triangular element by Zienkiewicz et al. [13] is used for out-of-plane deformation. Each node has six degrees of freedom, and the two elements are coupled with respect to the translational displacements. The number of elements for static analysis is 253. The shell has the uniform thickness of 0.1 m and is subjected to self-weight, which is supposed to be sufficiently small so that the deformation is small and the shell remains in the elastic range. The material of is supposed to be concrete with Young's modulus 21.0 kN/mm2, Poisson's ratio 0.17, and weight density 24.0 kN/m^3.

In each of the optimization problem formulated below, the total number of degrees of freedom, nodal displacement vector, linear stiffness matrix, total middle-surface area, and vector consisting of z-coordinates the supports are denoted by m, $\boldsymbol{d} \in R^m$, $\boldsymbol{K} \in R^{m \times m}$, S, and $\boldsymbol{r}^* \in R^6$, respectively. The value of initial shape is denoted by the subscript 0. The design variables are the z-coordinates $\boldsymbol{q}_z$ of the control points, because various shapes can be successfully represented by varying z-coordinates only.

5. 1. Minimization of strain energy without constraints on algebraic invariants

We first find the optimal shape without constraint on an algebraic invariant. The strain energy is minimized as follows under upper-bound constraint on the area:

$$\begin{aligned} &\text{minimize} && f(\boldsymbol{q}_z) = \frac{1}{2}\boldsymbol{d}^\top \boldsymbol{K}\boldsymbol{d} \\ &\text{subject to} && \begin{cases} S(\boldsymbol{q}_z) - S_0 = 0 \\ \boldsymbol{r}^*_z(\boldsymbol{q}_z) - \boldsymbol{r}^*_{z,0} = 0 \end{cases} \end{aligned} \tag{25}$$

The initial and optimal shapes are shown in Figures 2 and 3, respectively, and their mechanical performances are listed in the second and third columns of Table 1. It can be confirmed from the optimization result that the bending and tensile stresses are reduced and the shape is optimized so that the shell resists the self-weight mainly with compression.

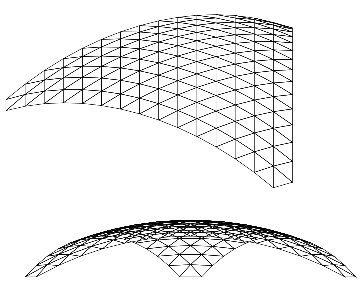

Figure 2 : Initial Shape of Model 1

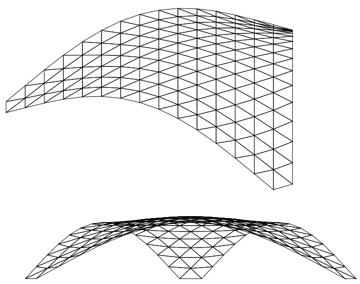

Figure 3 : Optimal shape of Problem (25)

5. 2. Minimization of strain energy under constraints on β-invariants

We next consider the following optimization problem by introducing the constraints on β-invariants to obtain a locally convex surface:

$$\begin{aligned} &\text{minimize} && f(\boldsymbol{q}_z) = \frac{1}{2}\boldsymbol{d}^\top \boldsymbol{K}\boldsymbol{d} \\ &\text{subject to} && \begin{cases} S(\boldsymbol{q}_z) - S_0 = 0 \\ \boldsymbol{r}^*_z(\boldsymbol{q}_z) - \boldsymbol{r}^*_{z,0} = 0 \\ \beta^c_2(\boldsymbol{q}_z) > \underline{0} \\ \beta^c_1(\boldsymbol{q}_z) \le \overline{\beta} \end{cases} \end{aligned} \tag{26}$$

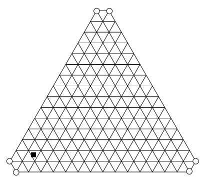

Point at which β-invariants are constrained

where $\overline{\beta} < 0$ ensures convexity around the point indicated by the filled square in the Figure. The values of the constrained point are denoted by the superscript c. Figures 4 and 5 show the optimization results for $\overline{\beta} = -0.1$ and 0.2, respectively. The mechanical properties are listed in the fourth and fifth columns of Table 1. As is seen, the maximum values of displacement, compressive stress, and bending stress increase as a result of assigning requirement of local convexity. The maximum displacement and stresses also increase as the absolute value of β^c_1 is increased to generate more locally convex surface.

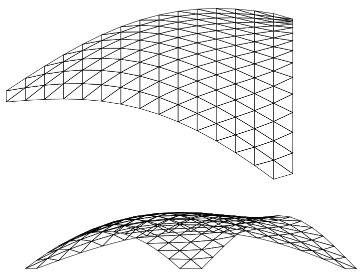

Figure 4 : Optimal shape of Problem (26) ($\overline{\beta} = -0.1$)

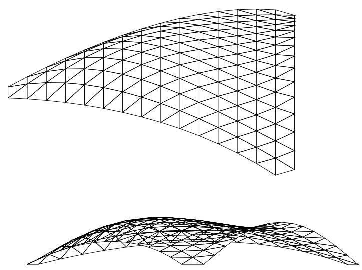

Figure 5 : Optimal shape of Problem (26) ($\overline{\beta} = -0.3$)

5. 3. Minimization of strain energy under constraints on γ-invariants

We next solve the following problem with constraints on γ-invariants to obtain locally cylindrical and concave surface:

$$
\begin{aligned}
&\text{minimize} \quad f(\boldsymbol{q}_z) = \frac{1}{2}\boldsymbol{d}^\top \boldsymbol{K}\boldsymbol{d} \\
&\text{subject to} \quad \begin{cases} S(\boldsymbol{q}_z) - S_0 = 0 \\ \boldsymbol{r}_z^*(\boldsymbol{q}_z) - \boldsymbol{r}_{z,0}^* = 0 \\ \gamma_2^{ci}(\boldsymbol{q}_z) = 0 \\ \gamma_3^{ci^2}(\boldsymbol{q}_z) - \gamma_1^{ci^2}(\boldsymbol{q}_z) > 0 \quad (i=1,2) \\ \gamma_3^{ci}(\boldsymbol{q}_z) \geq \overline{\gamma}^{ci} \end{cases}
\end{aligned}
\tag{27}
$$

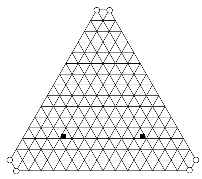

Point at which γ-invariants are constrained

where the constraints on the invariants are given at points $ci(i = 1, 2)$ indicated by the filled square in the Figure. Figures 6 and 7 show the optimization results for $\overline{\gamma}^{ci} = 0.004$ and 0.006, respectively. It can be confirmed that a locally cylindrical and concave surface has been successfully obtained by introducing the constraints on the γ-invariants. The maximum displacement and stresses listed in the last two columns of Table 1 also increase as the value of $\overline{\gamma}^{ci}$ is increased to generate more locally cylindrical and concave surface.

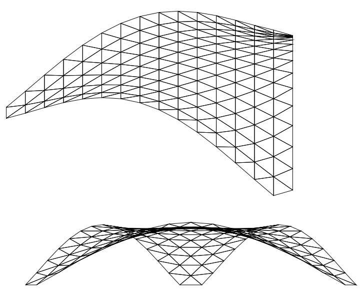

Figure 6 : Optimal shape of Problem (27) ($\overline{\gamma} = 0.004$)

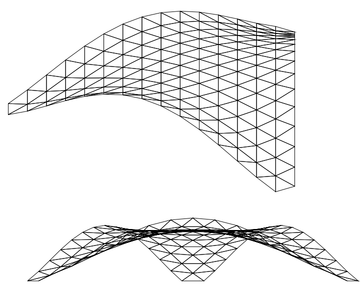

Figure 7 : Optimal shape of Problem (27) ($\overline{\gamma} = 0.006$)

Table 1 : Mechanical properties of initial and optimal shapes of Model 1

	Initial (Fig.2)	Without invariants (Fig.3)	$\overline{\beta} = -0.1$ (Fig.4)	$\overline{\beta} = -0.2$ (Fig.5)	$\overline{\gamma} = 0.004$ (Fig.6)	$\overline{\gamma} = 0.006$ (Fig.7)
Strain energy [kNm]	5.733	0.669	0.860	1.650	0.737	1.504
Max. vertical disp. [mm]	59.88	3.432	6.931	13.00	4.236	9.925
Max. compressive stress [N/mm^2]	3.600	2.613	2.926	4.129	2.978	5.780
Max. tensile stress [N/mm^2]	0.917	0.114	0.077	0.197	0.176	0.789
Max. bending stress [N/mm^2]	6.927	0.585	0.843	2.333	0.673	1.787

5. 4. Minimization of α-invariant and strain energy

Finally, we consider the following multiobjective optimization problem for minimizing the strain energy and sum of α-invariants at the 15 points indicated by filled square in the Figure:

$$
\begin{aligned}
&\text{minimize} \quad \begin{cases} f(\boldsymbol{q}_z) = \dfrac{1}{2}\boldsymbol{d}^{\top}\boldsymbol{K}\boldsymbol{d} \\ g(\boldsymbol{q}_z) = \displaystyle\sum_{i=1}^{15} \alpha^{ci} \end{cases} \\
&\text{subject to} \quad \begin{cases} S - S_0 = 0 \\ \boldsymbol{r}_z^* - \boldsymbol{r}_{z,0}^* = 0 \end{cases}
\end{aligned}
\tag{28}
$$

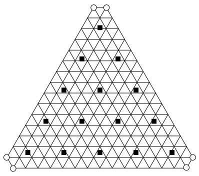

Point at which α-invariants are measured

To solve this problem using the constraint method for multiobjective programming, we convert the problem to the following two single-objective optimization problems:

$$
\begin{aligned}
&\text{minimize} \quad f(\boldsymbol{q}_z) \\
&\text{subject to} \quad \begin{cases} S(\boldsymbol{q}_z) - S_0 = 0 \\ \boldsymbol{r}_z^*(\boldsymbol{q}_z) - \boldsymbol{r}_{z,0}^* = 0 \\ g(\boldsymbol{q}_z) - \overline{g} \leq 0 \end{cases}
\end{aligned}
\tag{29}
$$

$$
\begin{aligned}
&\text{minimize} \quad g(\boldsymbol{q}_z) \\
&\text{subject to} \quad \begin{cases} S(\boldsymbol{q}_z) - S_0 = 0 \\ \boldsymbol{r}_z^*(\boldsymbol{q}_z) - \boldsymbol{r}_{z,0}^* = 0 \\ f(\boldsymbol{q}_z) - \overline{f} \leq 0 \end{cases}
\end{aligned}
\tag{30}
$$

where $\overline{g}$ and $\overline{f}$ are the upper bounds of the sum of α-invariants and the strain energy, respectively. The Pareto optimal solutions are found parametrically by solving Problem (29) for the region of large strain energy and Problem (30) for the region of large α-invariants, where the upper bound are parametrically varied. Figure 8 shows Pareto front and its mechanical properties, and Figures 9-11 show several Pareto optimal solutions with contour lines. The mechanical quantities are also shown Table 2. As is seen from these figures, the shell surface approaches a spherical surface as $g(\boldsymbol{q}_z)$ is decreased. Although the shape of optimal solution for $\overline{f} = 1.0$ is almost similar to the initial shape that has an almost spherical surface, the stiffness of the optimal shape is much larger than that of the initial shape. This way, a mechanically efficient surface consisting of truncated spherical surface can be generated by optimization.

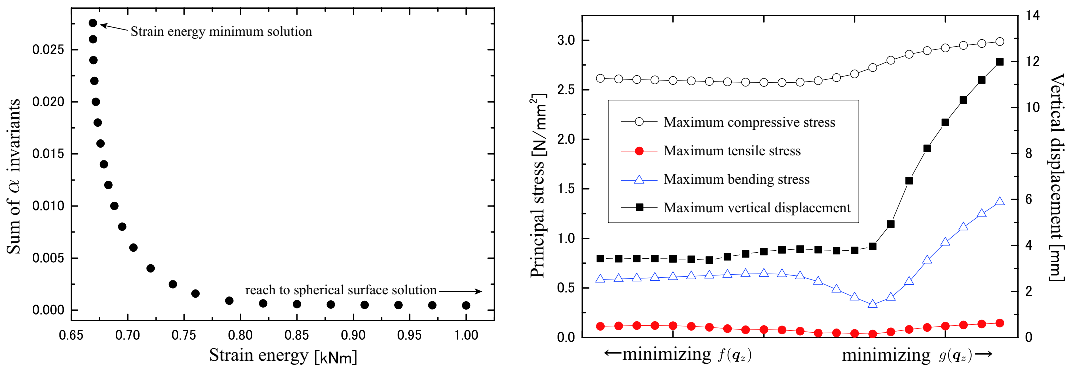

Figure 8 : Pareto front and its mechanical properties

Table 2 : Mechanical properties of several Pareto optimal solutions considering α-invariants and strain energy

	$\overline{g} = 0.02$ (Fig. 9)	$\overline{f} = 0.76$ (Fig. 10)	$\overline{f} = 1.00$ (Fig. 11)	Initial (Fig. 2)
Strain energy [kNm]	0.672	0.760	1.000	5.733
Sum of α invariants	0.020	1.6×10^3	4.5×10^4	2.9×10^6
Max. vertical disp. [mm]	3.419	3.783	11.99	59.88
Max. compressive stress [N/mm^2]	2.593	2.661	2.986	3.600
Max. tensile stress [N/mm^2]	0.118	0.041	0.145	0.917
Max. bending stress [N/mm^2]	0.611	0.404	1.367	6.927

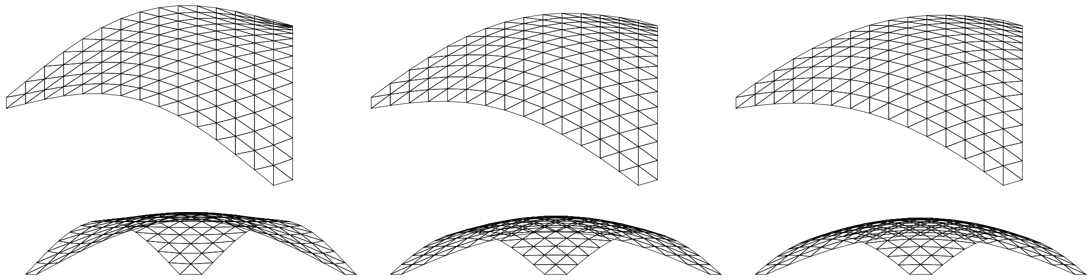

(a) elevation and diagonal view

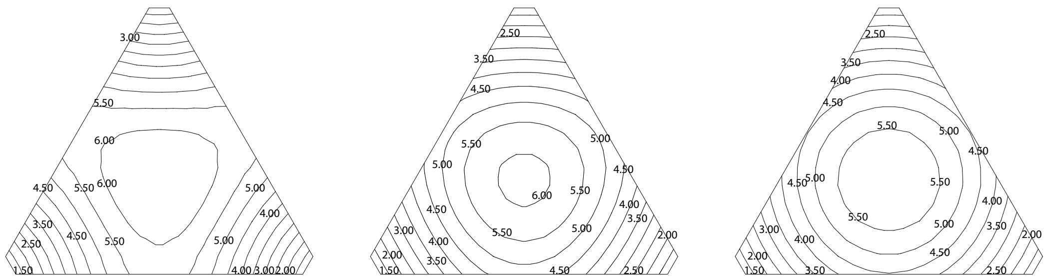

(b) contour line of vertical coordinates

Figure 9 : Optimal shape of Problem (29) ($\bar{g}$ = 0.02)

Figure 10 : Optimal shape of Problem (30) ($\bar{f}$ = 0.76)

Figure 11 : Optimal shape of Problem (30)($\bar{f}$ = 1.00)

6. Bézier surface with irregular plan

So far, we considered a surface with regular triangular plan. In this section, optimal shapes are found for the shell surface with irregular plan (Model 2) as shown in Figure 12, in order to demonstrate the effectiveness of using the triangular Bézier patch. The geometry of the control net is also shown in Figure 12. The rise is 8.0 m, and other parameters are the same as those of Model 1 in Sec. 5. The surface is modeled using ten triangular Bézier patches of order 4, and the design variables are the z-coordinates $\boldsymbol{q}_z$ of 52 control points as shown in the filled circle in Figure 12, where the symmetry conditions are utilized and the locations of supports are fixed. The structural analysis is carried out considering symmetry conditions. The continuity of gradient and curvature along the interior boundary between Bézier patches is not necessarily satisfied.

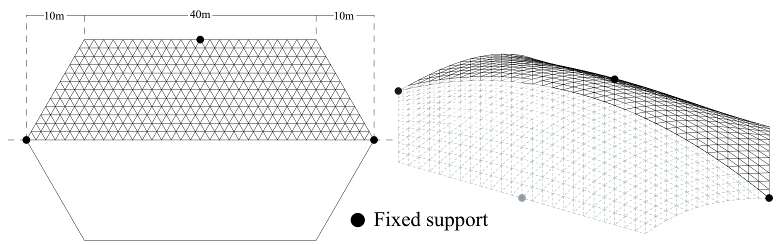

(a) plan and diagonal view

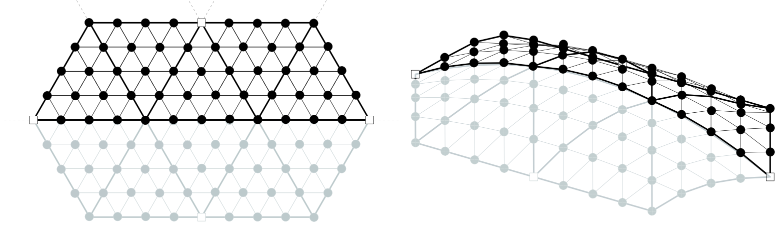

(b) Bézier patch and control points

Figure 12 : Shell surface with triangular plan (Model 2)

6. 1. Minimization of strain energy without constraints on algebraic invariants

We first find the optimal shape without constraint on an algebraic invariant. The following optimization problem is same as Problem (25):

$$\begin{aligned} &\text{minimize} && f(\boldsymbol{q}_z) = \frac{1}{2}\boldsymbol{d}^\top \boldsymbol{K}\boldsymbol{d} \\ &\text{subject to} && S(\boldsymbol{q}_z) - S_0 = 0 \end{aligned} \tag{31}$$

The initial and optimal shapes are shown in Figures 13 and 14, respectively. The mechanical quantities are also shown in the second and third columns of Table 3. It can be confirmed from the optimization results that the bending and tensile stresses are reduced and the shape is optimized so that the shell resists the self-weight mainly with compression in the similar manner as Model 1. However, the optimal shape depends on the load patters; therefore, multiple loading conditions should be considered for practical application. Note that the gradients are not continuous along the internal boundaries between the Bézier patches of the optimal shape. Globally smooth surface can be generated, if necessary, by assigning constraints on continuity of tangent vector (G^1-continuity) between two adjacent patches [14].

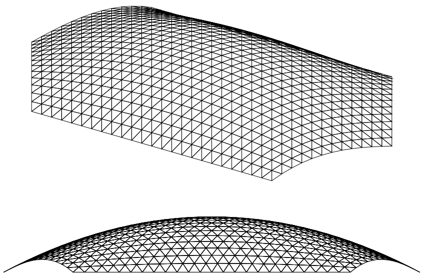

Figure 13 : Initial Shape of Model 1

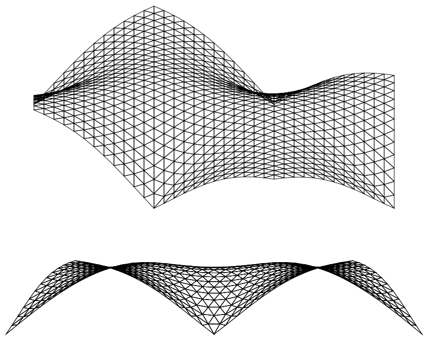

Figure 14 : Optimal shape of Problem (25)

6. 2. Minimization of strain energy under developability constraint

Next, we generate a developable surface by shape optimization. The following problem is to be solved so that β_2 vanishes at 105 points indicated by the filled squares in the Figure:

$$\begin{aligned} &\text{minimize} && f(\boldsymbol{q}_z) = \frac{1}{2}\boldsymbol{d}^\top \boldsymbol{K}\boldsymbol{d} \\ &\text{subject to} && \begin{cases} S(\boldsymbol{q}_z) - S_0 = 0 \\ \beta_2^{ci}(\boldsymbol{q}_z) = 0 \\ {\scriptstyle (i=1,\cdots,105)} \end{cases} \end{aligned} \tag{32}$$

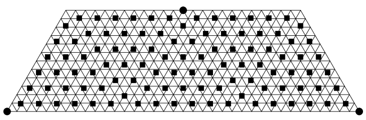

Points at which β-invariants are constrained

The optimal shape is shown in Figure. 15(a). Although β_2 is not guaranteed to vanish at the point where the constraint is not given, the contour lines became almost straight and parallel as shown in Figure 15(b), Hence, each of the 1/5 parts of the shell is nearly developable. Furthermore, both of the strain energy and maximum vertical displacement have smaller values than the initial shape as shown in the last column of Table 3. Note that a developable surface cannot be generated if continuity of gradient is assigned along the internal boundaries.

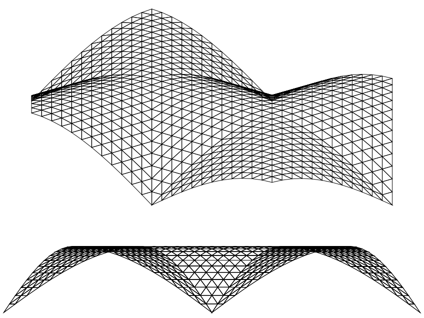

(a) elevation and diagonal view

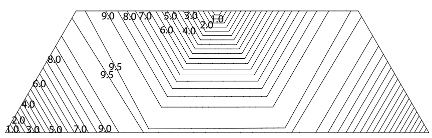

(b) contour line of vertical coordinates

Figure 15 : Optimal shape of Problem (25)

Table 3 : Mechanical properties of initial and optimal solutions

	Initial (Fig. 13)	Without invariants (Fig. 14)	With developability condition (Fig. 15)
Strain energy [kNm]	26.27	5.475	5.685
Max. vertical disp. [mm]	47.10	3.719	4.683
Max. compressive stress [N/mm^2]	16.22	8.266	8.500
Max. tensile stress [N/mm^2]	3.543	0.299	0.311
Max. bending stress [N/mm^2]	9.941	0.420	0.584

7. Conclusions

The local properties of the shell surface can be explicitly controlled by solving an optimization problem with constraints on the algebraic invariants of the surface. Nonlinear programming can be efficiently used because the sensitivity coefficients of invariants with respect to the locations of control points are explicitly derived. Furthermore, a developable surface can be obtained by assigning the constraint such that the Gaussian curvature vanishes everywhere on the surface. The trade-off relation between roundness and stiffness of the shell has been investigated using the constraint approach of multiobjective programming.

Hence, it may be concluded that the algebraic invariants are effective indices representing the local properties of the surface, and the optimal shell shape considering the aesthetic aspects, constructability and mechanical rationality can be generated using the proposed approach at the early design stage.

References

[1] S. Guillet, F. Noël, and J. C. Léon. Structural shape optimization of parts bounded by free-form surfaces. *Structural Optimization*, 11:159–169, 1996.

[2] E. Ramm, K.-U. Bletzinger, and R. Reitinger. Shape optimization of shell structures. *Bulletin of Int. Assoc. for Shell and Spatial Struct.*, 34(2):103–121, 1993.

[3] T. Kimura and H. Ohmori. Computational morphogenesis of free form shells. *J. Int. Assoc. Shells and Spatial Struct*, 49(3):175–180, 2008.

[4] L. Piegl and W. Tiller. *The NURBS Book*. Springer, Berlin, 1996.

[5] M. P. Bendsøe and O. Sigmund. *Topology Optimization: Theory, Methods and Applications*. Springer, 2003.

[6] M. Ohsaki, T. Nakamura, and M. Kohiyama. Shape optimization of a double-layer space truss described by a parametric surface. *Int. J. Space Struct.*, 12(2):109–119, 1997.

[7] M. Ohsaki and M. Hayashi. Fairness metrics for shape optimization of ribbed shells. *J. Int. Assoc. Shells and Spatial Struct.*, 41(1):31–39, 2000.

[8] M. Ohsaki, T. Ogawa, and R. Tateishi. Shape optimization of curves and surfaces considering fairness metrics and elastic stiffness. *Struct. Multidisc. Optim.*, 24:449–456, 2003, Erratum: Vol. 27, 250–258, 2004.

[9] S. Fujita and M. Ohsaki. Shape optimization of shells considering strain energy and algebraic invariants of parametric surface. *J. Struct. Constr. Eng., AIJ*, 74(639):841–847, 2009. (in Japanese).

[10] M. Iri, Y. Shimakawa, and T. Nagai. Extraction of invariants from digital elevation data with application to terrain topography. *Nonlinear Analysis*, 47:5585–5598, 2001.

[11] P. Gill, W. Murray, and M. Saunders. *User's Guide for SNOPT Version 7: Software for Large-Scale Nonlinear Programming*. Stanford Business Software Inc., 2008.

[12] O. C. Zienkiewicz. *The Finite Element Method in Engineering Science*. McGraw-Hill, 1971.

[13] G. P. Bazeley, Y. K. Cheung, B. M. Irons, and O. C. Zienkiewicz. Triangular elements in plate bending – conforming and nonconforming solutions. In *Proc. First Conference on Matrix Methods in Structural Mechanics*, pages 547–576, 1966.

[14] D. Wen-Hui and F. J. M. Schmitt. On the G^1 continuity of piecewise Bézier surfaces: A review with new results. *Computer-Aided Design*, 22(9):556–573, 1990.